

# Elementary reaction modeling and experimental characterization of solid oxide fuel-assisted steam electrolysis cells

Yu Luo<sup>a,b</sup>, Yixiang Shi<sup>a,\*</sup>, Wenying Li<sup>a</sup>, Meng Ni<sup>b,\*</sup>, Ningsheng Cai<sup>a</sup>

<sup>a</sup> Key Laboratory for Thermal Science and Power Engineering of Ministry of Education, Tsinghua

University, Beijing 100084, China

<sup>b</sup> Building Energy Research Group, Department of Building and Real Estate, The Hong Kong

Polytechnic University, Hung Hom, Kowloon, Hong Kong, China

## Abstract

A one-dimension elementary reaction kinetic model for solid oxide fuel-assisted steam electrolysis cell (SOFEC) is developed coupling heterogeneous elementary reactions, electrochemical reaction kinetics, electrode microstructure and transport processes of charge and mass. This model is calibrated and validated by experimental data from a button cell with anode gases of H<sub>2</sub>, CO and CH<sub>4</sub> at 800°C. After comparisons with solid oxide electrolysis cell (SOEC), the energy demands, performance and efficiency of CO-assisted SOFEC and CH<sub>4</sub>-assisted SOFEC are investigated numerically. One important finding is that over 80% of electricity can be saved by SOFEC at a current density of 3000 A.m<sup>-2</sup>. SOFEC assisted by CO or CH<sub>4</sub>

---

\* Corresponding author. Tel.: +86-10-62789955; Fax: +86-10-62789955.

Email: [shyx@tsinghua.edu.cn](mailto:shyx@tsinghua.edu.cn).

\* Corresponding author. Tel.: +852-27664152; Fax: +852-27645131.

Email: [bsmengni@inet.polyu.edu.hk](mailto:bsmengni@inet.polyu.edu.hk), [memni@graduate.hku.hk](mailto:memni@graduate.hku.hk).

for steam electrolysis has better performance than SOEC, especially by CH<sub>4</sub>. The efficiencies of 12%CO-SOFEC and 12%CH<sub>4</sub>-SOFEC are at least respectively 7% and 30% higher than that of SOEC at 800°C with the current density of below 2500 A.m<sup>-2</sup>. Finally, the effects of type of assisting-fuel, fuel composition and applied voltage are studied. It is found that CO-SOFEC shows higher anode polarization and thus lower performance than CH<sub>4</sub>-SOFEC with the same molar fraction of fuel. It's also found that the performance of SOFEC increases with increasing proportion of assisted fuel in anode at high current density.

**Keyword:** solid oxide fuel-assisted electrolysis cell(SOFEC); lower open-circuit voltage(OCV); efficiency; performance; elementary reaction model; carbon monoxide; methane.

## **Introduction**

The use of fossil fuels as the major energy source leads to increasingly more and more serious energy crisis and environmental issues such as global warming, air pollution and acid rain. To address these global issues, it is urgent to adopt clean and sustainable energy technologies. Renewable energies like solar energy and wind energy can perfectly meet our requirements as they are clean, sustainable, and abundant. However, renewable power is restricted in time and space, intermittent and site-specific, thus are not reliable for instantaneous supply of energy.[1] Electrolysis

technology can convert electrical energy to chemical energy regardless of the instability of renewable power. Hydrogen is an ideal and stable gas for storing chemical energy due to pollution free, which can be produced by electrochemically splitting water. And when demanded, hydrogen can release a large amount of energy by chemically or electrochemically oxidized back into water. Therefore, hydrogen is regarded as one of a potential alternatives for fossil fuels[2]. High temperature electrolysis (HTE) can utilize industrial waste heat, significantly reduce electrical consumption and improve reaction rate. Solid oxide electrolysis cell (SOEC) operated in the range of 600-1000°C is employed for HTE and widely studied.

Although part of electrical demand is replaced by more heat demand in high temperature SOEC, electricity is still the major energy consumption. However, electricity is a high-quality and expensive energy. As a result, the price of hydrogen production by electrolysis is 2-3 times higher than that of conventional steam reforming[2,3]. In addition, unsteady and intermittent power from renewable energy sometimes would limit the hydrogen production rate. To produce hydrogen steadily, extra electricity should be added from the grid, which mainly comes from the fossil fuel. Since fossil fuel is the major carbon emitter, the steam electrolysis process with extra electricity from grid is not absolutely carbon-free.

Solid oxide fuel-assisted electrolysis cell (SOFEC) is a novel approach for electrolysis. Compared with SOEC, SOFEC consumes much less electricity, thus the hydrogen production characteristics is less dependent on the electrical energy input. Similar with SOEC, steam is fed into cathode in a SOFEC. Different from SOEC, fuel

is fed and oxidized in anode of SOFEC. The half cell reaction in cathodes of both SOEC and SOFEC is:



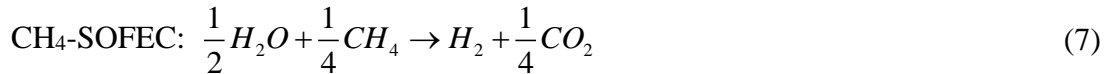
The half cell reaction in anode of SOEC is:



As for SOFEC using CO and CH<sub>4</sub> as assisting-fuel, the half cell reactions in anode (when fully oxidized) are respectively:



The total cell reactions of SOEC and SOFEC are respectively:



Clearly, the working principle of SOFEC is actually a reforming reaction in an electrochemical way. Thermodynamically, adding assisting-fuel significantly decreases the total energy demand. Therefore, the electrical energy can also be greatly saved even completely replaced when steam is electrolyzed by SOFEC.

Theoretically, the open-circuit voltage (OCV) can be determined by the reversible Nernst potential representing the minimum of electrical demand. The theoretical reversible potential of SOFEC is at least 1V lower than that of SOEC. Assuming that irreversible losses in SOFEC are identical to SOEC, a large amount of electricity can be saved by adding relatively cheaper fuels, such as carbon, carbon

monoxide, nature gas, biomass and other hydrocarbon fuels.

The cell power density can be calculated as:

$$P(W.m^{-2}) = i(A.m^{-2}) \cdot V \quad (8)$$

Generally, the OCV of SOFEC is negative. When  $V_{OCV} < V < 0$ , the power density is negative, that is, SOFEC can not only produce hydrogen but also generate electricity. In this voltage range, irreversible losses of SOFEC are not too large so that chemical energy from assisting fuel is higher than the electrical demand. When  $V > 0$ , power density turns positive, indicating that irreversible losses are higher than the chemical energy from the assisting fuel. When  $V = 0$ , power density is equal to zero, meaning that SOFEC generates hydrogen without any electricity input or output.

A patent about this novel method was applied by Pham et al. in 2000, which demonstrated this principle using natural gas fed to the anode of SOEC. [4] Since that, this method has aroused much interest in researchers. Experiments on single natural-gas-assisted cells by Martinez-Frias et al. showed a voltage reduction of as much as 1V when compared to conventional steam electrolyzers[2]. The performance of various anodes was then tested by Wang et al. in a SOEC for the conditions where the anode was exposed to the reducing gases  $H_2$ ,  $CH_4$  and  $CO$ . Pd-C-CeO<sub>2</sub>-YSZ showed the highest catalytic activity and gave the largest reductions in the OCV of the SOE cell. [5] And direct oxidation of methane dominates and resulting in a higher ASR at low  $CH_4$  conversions. [6] At system level, analysis of Martinez-Frias et al. indicates incorporating the electrolyzer with a heat recovery system (heat exchangers and catalytic reactor) results in a high-efficiency hydrogen production system. The

system efficiency is up to 70% with respect to primary energy. [2] Tao et al. build an SOFC-SOFEC hybrid unit for hydrogen and electrical energy generation that is able to produce several hundred watts of electrical power and pure hydrogen simultaneously. [7]

Although many researchers pay attention to SOFEC, most researches are experimental studies with a focus on performance evaluation and system design. A validated mechanism model combined with experiment is helpful to understand the complex reacting and transport phenomena in SOFEC, as relevant information is hard to obtain by experiments. In this paper, an elementary reaction kinetic model of SOFEC was developed, coupling heterogeneous elementary reactions, electrochemical reactions, electrode microstructure, and transport processes of mass and charge. Compared to common thermal chemical modeling, the elementary reaction modeling fully considers each elementary reaction steps, which offers more detailed information of the reaction steps on the catalyst surface. This model was calibrated and validated with the experimental data for a SOFEC button cell at 800°C. Based on this one-dimension model, parametric simulations are conducted to compare the energy demands, performance and efficiency of SOEC, CO-assisted SOFEC and CH<sub>4</sub>-assisted SOFEC. Finally, SOFECs assisted by CO and CH<sub>4</sub> are compared and the effect of fuel composition and applied voltage are discussed.

## 2. Model Development

### 2.1 Model assumption and geometry

The model is built based on a button cell tested in our group. The assumptions are listed as follows:

- (1) All gases are assumed to be ideal gases.
- (2) Because of the 730  $\mu\text{m}$  cell thickness, the temperature within the cell is uniform so that all model parameters can be evaluated at a given temperature.
- (3) The convection flux and pressure gradient in the porous electrodes are neglected.
- (4) The reaction kinetic mechanism in anode is modeled using a set of elementary reactions that represent chemical reactivity at the molecular scale. The heterogeneous chemical and electrochemical reactions are assumed to only take place respectively on the Ni surface and directly at the triple-phase boundary (TPB). That's to say, Ni is used as catalyst, and the active sites for all heterogeneous reactions involving gas adsorption or desorption and surface reactions only exist on the Ni surface.
- (5) All surface species on the Ni surface are considered to be uncharged and the charge transfer reactions are assumed to take place in one step.
- (6) Continuum medium model is adopted. The distributions of electronic and ionic conductors in electrodes are assumed to be uniform and continuous, and the electrodes are isotropic media with stable and porous microstructures. The effect of carbon deposition on the pore structure and reaction activities in anode is

ignored.

(7) Mean field approximation is employed for anode heterogeneous reactions, thus the surface adsorbates distribute uniformly over the catalyst surface.

(8) The high purity platinum is applied as the cathode, which conducts electrons only.

Thus, the TPB only exist at the interface of cathode and electrolyte, assumed to be a 1 $\mu$ m thick domain. (as Fig. 1 shows)

(9) For simplicity, the non-uniformity in the radial direction is neglected.

Based on the assumptions, the button cell is predigested to a 1D model along the thickness direction. Fig. 1 shows the model structures, calculation domains and boundaries of fuel-assisted steam electrolysis. The materials of electrodes and electrolyte in the model are the same as the button cell tested so that this model is more feasible and reflects the real situation more closely. In this model, heterogeneous chemistry, electrochemistry, charge balance and mass balance are all considered and explained below.

**Fig. 1 Model structures, calculation domains and boundaries of fuel-assisted steam electrolysis.**

## **2.2 Anode heterogeneous chemistry**

In Ni/YSZ anode, Ni is not only electronic conductor but also an efficient catalyst of surface reactions. In common thermal chemical modeling, various overall reactions are modeled independently using kinetic expressions. The important



interaction between different reactions cannot be included in the thermal chemical modeling, such as the competitive adsorption of the species on the catalyst surface. It's difficult to determine the chemical or electrochemical reaction processes, especially for methane. With Ni-based catalyst, a heterogeneous reaction mechanism was developed and evaluated at 800°C by Ethan et al.[8]. They proposed 42 elementary reactions including 6 adsorptions, 6 desorptions and 30 surface reactions and involving 5 gas species and 12 surface-adsorbed species. Based on the work of Ethan et al, Janardhanan and Deutschmann used an extended mechanism which is applicable to a large temperature range of 220°C to 1700°C[9], as shown in Table 1. The mechanism has simultaneously considered many processes including reversible water-gas shift reactions, reversible methane-steam reforming reactions and surface carbon coverage. This mechanism can be simplified and widely employed for not only SOFC fueled with CO, H<sub>2</sub>, syngas and CH<sub>4</sub>, but also SOEC for electrolysis of H<sub>2</sub>O and CO<sub>2</sub> and co-electrolysis of H<sub>2</sub>O and CO<sub>2</sub>. [8-13] The structures and materials of the anode in SOFEC are completely same as those of the anode in SOFC[10,11]. Thus, the mechanism is adopted to analyze the reaction kinetics of H<sub>2</sub>, CO and CH<sub>4</sub> in the SOFEC model.

**Table 1 Heterogeneous reaction mechanism on Ni-based catalysts[8,9]**

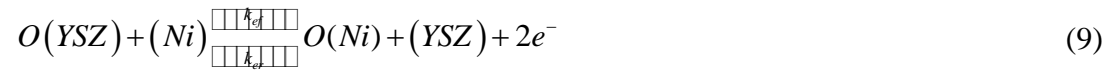
The equations related to anode heterogeneous chemistry are summarized in Table 2. The detailed explanation and description can be found in our previous papers [10-15] The effective Ni surface area per unit volume ( $S_{Ni}$ ) is based on the particle coordination number theory in binary random packing of spheres and the percolation

theory.[16,17]

## Table 2 Equations for anode heterogeneous chemistry

### 2.3 Electrochemistry

For the consistency of electrochemical and heterogeneous reactions, anode charge transfer reaction is one-step, which needn't consider the respectively electrochemical oxidization of H<sub>2</sub>, CO and CH<sub>4</sub>. The one-step charge transfer reaction can be written as [19]:



O(YSZ) denotes the oxygen interstitial and (YSZ) denotes the oxygen vacancy in the YSZ ionic conductor.  $k_{ef}$ ,  $k_{er}$  are respectively the forward and reversed charge transfer reaction rate constant. Similar to Butler-Volmer equation,  $k_{ef}$  and  $k_{er}$  can be expressed as:[10,19]

$$k_{ef} = \frac{i_{0,an}}{2Fc_{O(YSZ)}^0 c_{(Ni)}^0} \exp\left[-\frac{2(1-\alpha_{an})F\eta_{an}}{RT}\right] \quad (10)$$

$$k_{er} = \frac{i_{0,an}}{2Fc_{O(Ni)}^0 c_{(YSZ)}^0} \exp\left[-\frac{2(1-\alpha_{an})F\eta_{an}}{RT}\right] \quad (11)$$

where  $i_0$  denotes the exchange current density and  $c^0$  denotes the species surface concentrations at equilibrium state.  $\alpha$  is the charge transfer coefficient, and  $\eta_{an}$  denoting the anode overpotential can be expressed as:

$$\eta_{an} = V_{elec,an} - V_{ion,an} - V_{ref,an} \quad (12)$$

$V_{elec}$ ,  $V_{ion}$  are respectively the electronic and ionic potential at the TPB interface, which were calculated by charge balance equations in Table 3.  $V_{ref}$  is equal to ( $V_{elec} - V_{ion}$ ) at

equilibrium state. Similarly to anode overpotential, the expression of cathode overpotential is given:

$$\eta_{ca} = V_{elec,ca} - V_{ion,ca} - V_{ref,ca} \quad (13)$$

In this model,  $V_{ref,an}$  is set to zero so that  $V_{ref,ca}$  is equal to actual OCV. The anode overpotential  $\eta_{an}$  and cathode overpotential  $\eta_{ca}$  mainly denote activation overpotentials in anode and cathode, which are used to provide energy for charge-transfer reaction. In the anode,  $\eta_{an}>0$  denoting the charge-transfer reaction is negative and producing electrons. In the cathode,  $\eta_{ca}<0$  denoting charge-transfer reaction is positive and consuming electrons. The anode current source term is expressed as:

$$Q_{elec,an} = -Q_{ion,an} = 2F \left( k_{ef} c_{O(YSZ)} c_{(Ni)} - k_{er} c_{O(Ni)} c_{(YSZ)} \right) S_{TPB,an} \quad (14)$$

$S_{TPB}$  denotes the effective TPB areas, where charge transfer reactions occur. In the anode, TPB exist at the interface of nickel and ionic conductors, which can be well evaluated through the micro Monte Carlo model developed by Zhang et al.[20-22]. By giving the particle radius distributions of electronic conductors and ionic conductors, a 3D microstructure of electrode can be constructed and the length of TPB  $L_{TPB,an}(m \cdot m^{-3})$  also can be calculated accurately. It should be noted that the anode contains anode support layer and anode active layer. The anode support layer has larger particles than anode active layer, so  $L_{TPB}$  in the two layers should be calculated separately. The width of TPB  $W_{TPB}(m)$  can be calculated by the following expression:

$$W_{TPB} = (r_{elec} + r_{ion}) (1 - \cos \theta) \quad (15)$$

where  $r_{elec}$ ,  $r_{ion}$  are respectively the mean particle radiuses of electronic and ionic

conductors,  $\theta$  denoting the contact angle is set as  $15^\circ$ . [16]. Thus, the area of TPB in the anode can be calculated by the expression:

$$S_{TPB,an} = W_{TPB} L_{TPB} \quad (16)$$

The Butler-Volmer equation is employed to express the cathode current source term [16]:

$$Q_{elec,ca} = -Q_{ion,ca} = i_{0,ca} L_{TPB,ca} \left[ \frac{c_{H_2}^{TPB}}{c_{H_2}^{bulk}} \exp\left(\frac{2\alpha_{ca} F \eta_{ca}}{RT}\right) - \frac{c_{H_2O}^{TPB}}{c_{H_2O}^{bulk}} \exp\left(-\frac{2(1-\alpha_{ca}) F \eta_{ca}}{RT}\right) \right] \quad (17)$$

Differing from anode, the Pt cathode only conducts electrons and thus TPB only exist at the interface of cathode and electrolyte. The  $L_{TPB}(\text{m.m}^{-2})$  in cathode can be evaluated by the following expression. [23]

$$L_{TPB,ca} = 2\pi r_{elec} \sin \theta (n n_{elec})^{2/3} \quad (18)$$

$n$  is the particle number per volume,  $n_{elec}$  denoting the number fraction of electronic conductors is equal to 1 since only Pt is used.

## 2.4 Governing Equations

The governing equations for charge balance and mass balance are summarized in Table 3, which have been described in details in our previous work [10-15]. The extended Fick's model (EFM) considering Knudsen diffusion and molecular diffusion [17,18,24,25] is adopted to simulate the mass transfer in the porous electrodes.

### Table 3 Governing equations for charge balance and mass balance

## 2.4 Boundary conditions

On the basis of the operation conditions and model simplifications, the boundary conditions of charge and mass balances partial differential equations are listed in Table 4. The boundary condition “insulation” signifies that the partial derivative is zero and “continuity” signifies that the variables are continuous at the boundary.  $V_{\text{cell}}$  denotes the applied voltage and  $c_{\text{g,an}}$ ,  $c_{\text{g,ca}}$  denote the molar concentrations of gas species fed in the anode and cathode, respectively.

### Table 4 Boundary conditions

## 2.5 Model parameters

Table 5 lists the pore structure parameters in porous electrode and Table 6 lists the values or expressions of materials properties and other parameters, which have been described in detail in previous papers [11,14]. The pore structure of anode support layer was characterized using mercury porosimeter. (Micromeritics AutoPore IV, USA) The mean pore diameter and porosity were found to be 0.387  $\mu\text{m}$  and 0.335, respectively. To simplify the calculation, the mean particle diameters of the two conductors are assumed to be the same and equal to the mean pore diameter [27]. The same measuring method is very difficult to characterize the pore structures of cathode and anode active layers since these two layers are thin and hard to be separated from the cell. Thus, the pore size and porosity of each layer were determined by comparing SEM images based on quantitative stereology [14]. The results showed that the

average pore diameter of anode active layer and cathode layer was about 1.5 and 1.2 times smaller than that of anode support layer, but the porosities of all three layers were almost the same. Some model parameters are not available from the published literature or by experimental measurement in our group, which are thus used as tuning parameters in model calibration and validation. Tuning parameters are listed in “Model calibration and validation” section.

**Table 5 Pore structure parameters in porous electrode**

**Table 6 Properties and parameters for model calculation**

## **2.6 Model solution method**

The finite element commercial software COMSOL MULTIPHYSICS® is employed for model calculation. The SOFEC button cell performance was calculated at a given cell voltage  $V_{\text{cell}}$ . For 1D SOFEC model, the maximum of ionic current density at a given cell voltage was obtained in the electrolyte layer. A complete polarization curve can be simulated by varying the cell voltage.

## **3. Experiment**

### **3.1 SOFEC button cell under test**

Anode-supported SOFEC button cells fabricated by Shanghai Institute of Ceramics Chinese Academy of Sciences were utilized in this research. The button cell

consists of four layers: a Ni-YSZ anode support layer (680  $\mu\text{m}$ ), a Ni-ScSZ anode active layer (15  $\mu\text{m}$ ), a ScSZ electrolyte layer (20  $\mu\text{m}$ ) and a Pt cathode layer (15  $\mu\text{m}$ ), as shown in Fig. 1. The Pt cathode layer with 13mm diameter was screen-printed on the electrolyte. The diameters of anode and electrolyte were both 26mm. In addition, a reticular silver layer was screen-printed on the anode for current collection.

### **3.2 Testing procedure**

A button cell reactor and an experimental measurement system were built for evaluating the cell performance and characterizing exhaust gas compositions, which is shown in details in our previous work [11,14]. A water bath was adopted to add a certain ratio of steam into the inflow gas. The steam amount and content were adjusted by the carrier gas amount and the temperature of the waterbath. The steam content was measured by a humidity transmitter (Testo6681, Germany) and calibrated by measuring the weight increase of calcium chloride anhydrous desiccant within 0.5 to 2 h.

Before testing, pure  $\text{H}_2$  was sent into the reactor for 1 h at  $800^\circ\text{C}$  to reduce the anode. The operating temperature was kept at  $800^\circ\text{C}$  during the whole experiment. The humidified gases with separately 97% $\text{H}_2$ , 97% $\text{CO}$  and 3% $\text{CH}_4$  were fed into anode and the gas with 20% steam (80% Ar as carrier gas for safe and stable operation) inflows cathode. The details of operating condition are shown in Table 7.

#### **Table 7 Operating condition of SOFEC experiment**

## **4. Results and discussion**

### **4.1 Model calibration and validation**

After calibrated and validated by the experimental data obtained for the conditions listed in Table 7, the simulated polarization curves with H<sub>2</sub>, CO and CH<sub>4</sub> fed separately in anode are compared with the experimental curves (Fig. 2). Despite of favorable OCV, large overpotential loss was observed for SOFEC assisted by CH<sub>4</sub>. This could be caused by carbon deposition from CH<sub>4</sub>, which could block the active sites for chemical or electrochemical reactions, further causing low cell performance. In order to eliminate the effect of carbon deposition on pore structure and reaction sites (Assumption 6), anode gas with 3% CH<sub>4</sub> is chosen to calibrate the model. According to Fig. 2, the modeled polarization curves agree well with the experimental data, which illustrates this model can reflect the actual phenomena in SOFEC. By means of the experimental curves, the determined values of tuning parameters are shown in Table 8.

**Fig. 2 Simulated and experimental polarization curves of SOFEC assisted by H<sub>2</sub>, CO and CH<sub>4</sub> at 800°C.**

**Table 8 Model tuning parameters**



## 4.2 Comparison of energy demand and efficiency between SOEC and SOFEC

### 4.2.1 Thermodynamic analysis of SOEC and SOFEC

On the thermodynamics of electrochemistry, Gibbs free energy change  $\Delta G$  denotes electricity demand and heat demand is depended on  $T\Delta S$ , where  $S$  is the entropy. Enthalpy change  $\Delta H$  is the sum of  $\Delta G$  and  $T\Delta S$ , denoting total energy demand. The theoretical energy demands of steam electrolysis by SOEC and CO or CH<sub>4</sub> assisted SOFEC in the temperature range of 100°C to 900°C are drawn in Fig. 3. The heat demand curves of SOEC and CH<sub>4</sub>- assisted SOFEC (CH<sub>4</sub>-SOFEC) are specially pointed out in the figure because they almost overlap with each other. Fig. 3 indicates that SOEC demands 200 kJ.mol<sup>-1</sup> more electricity than SOFEC assisted by CO or CH<sub>4</sub>. The electricity demand of CO- assisted SOFEC (CO-SOFEC) increases with increasing temperature, while that of CH<sub>4</sub>-assisted SOFEC decreases. When temperature is over 600°C, CH<sub>4</sub>-SOFEC theoretically doesn't demand electricity. But CO-SOFEC starts to demand electricity when temperature is over 820°C. As for heat, CH<sub>4</sub>-SOFEC has similar heat demand with SOEC. For comparison, CO-SOFEC doesn't demand heat but release heat in the considered temperature range. The efficiencies considering both heat and electricity is discussed in the Section 4.2.3.

**Fig. 3 Energy demands of steam electrolysis by SOEC and CO or CH<sub>4</sub> assisted SOFEC from 100°C to 900°C**

#### 4.2.2 The performance and electrical demands of SOEC and SOFEC

The performance of electrolysis process can be primarily characterized by the overpotential obtained from polarization curves. Large overpotential means large irreversible losses and thus poor cell performance. The SOEC model of Li et al.[13] developed in our previous work and validated by the experimental data from the same button cell is adopted to generate the polarization curve simulated for a comparable condition. The modeled conditions of SOEC, CO-SOFEC and CH<sub>4</sub>-SOFEC are listed in Table 9. Ar is used as carrier gas. The simulated polarization curves (i-V curves) and power density vs current density curves (i-P curves) are shown in Fig. 4. Polarization curves indicate that the performances of SOFEC assisted by 12%CH<sub>4</sub> and 12%CO are similar. The overpotentials of SOFECs are lower than that of SOEC and gradually approached even surpassed by that of SOEC with increasing current density due to the lack of assisting fuel. When the assisting fuel is insufficient, increasing overpotentials of SOFEC lead to larger irreversible loss and less advantage. Whether the synthetic effect of adding assisting fuel is positive or negative can be judged by efficiency comparison made in Section 4.2.3. The power demand considering thermodynamics and reaction kinetics in Fig. 4 includes reversible and irreversible electrical consumption, which is different from those in thermodynamic analysis part (Section 4.2.1) just denoting reversible electrical consumption and ignoring the irreversible losses. Therefore, the i-P curves show the actual power demands of various steam electrolysis processes. 12%CO-SOFEC doesn't demand electricity input until the current density is more than 1200 A.m<sup>-2</sup>, while 12% CH<sub>4</sub>-SOFEC starts

to demand electricity at the current density of over  $1750 \text{ A.m}^{-2}$ . For comparison, the power demand of SOEC increases rapidly with the increase of current density. At the current density of  $3000 \text{ A.m}^{-2}$ , the power demand of SOEC reaches  $5800 \text{ W.m}^{-2}$  while CO-SOFEC and CH<sub>4</sub>-SOFEC just require respectively  $1150 \text{ W.m}^{-2}$  and  $650 \text{ W.m}^{-2}$ . In this case, over 80% of electricity can be saved with CO or CH<sub>4</sub> assisted SOEC.

#### **Table 9 Simulated condition of SOEC, CO-SOFEC and CH<sub>4</sub>-SOFEC**

**Fig. 4 The i-V and i-P curves of SOEC, 12%CO-SOFEC and 12%CH<sub>4</sub>-SOFEC**

#### 4.2.3 The efficiency of SOEC and SOFEC

There is no doubt that plenty of electricity can be replaced by the chemical energy from the assisting fuel of SOFEC. However, it's possible that this process causes much more losses and a considerable amount of chemical energy from fuel is transformed into heat instead of electricity. Whether the total energy consumption of SOFEC is less than that of SOEC is still unknown. Thus, it is necessary to evaluate and compare the efficiencies of SOEC and SOFEC. Fig. 5 shows the energy transfer processes in SOEC and SOFEC. SOEC produces hydrogen from heat and electricity and meanwhile releases a part of heat owing to mainly polarization losses. As for SOFEC, fuel is consumed to produce hydrogen and a little electricity when  $V < 0$ , and fuel and electricity are consumed to product hydrogen when  $V > 0$ . Moreover, irreversible heat always exists due to various overpotential losses. The reversible heat is released in CO-assisted SOFEC but demanded in CH<sub>4</sub>-assisted SOFEC, which has

been analyzed in Section 4.2.1.

**Fig. 5 The energy transfer processes of SOEC and SOFEC**

Based on the 1D button cell model, the efficiency analysis is performed at 800°C. Assuming non-uniform temperature and gas composition, the expression of each energy form is given in Table 10. For comparison's sake, stoichiometric coefficient of hydrogen in each total reaction is set to 1 to guarantee that the charge transfer number  $n$  in each total reaction is 2.

**Table 10 The energy expressions of energy forms in SOEC and SOFEC**

4.2.3.1 The efficiency ignoring heat

As known, the industrial waste heat is abundant and heat is a low-quality form of energy. When the heat demand is neglected, only electrical energy and chemical energy in fuel and hydrogen should be considered. Therefore, the efficiencies of SOEC, CO-SOFEC and CH<sub>4</sub>-SOFEC can be expressed as the equations shown in Table 11. Combining the expressions and polarization curves, the efficiency vs current density curves (or hydrogen production rate) at 800°C are drawn as Fig. 6. Because CH<sub>4</sub> has lower Lower Heating Value (LHV, 200.2 kJ per mole H<sub>2</sub>O generated) than CO (282.4 kJ.mol<sup>-1</sup>) and H<sub>2</sub> (248.3 kJ.mol<sup>-1</sup>), highest efficiency of all is achieved when CH<sub>4</sub> is used for assisting steam electrolysis. The efficiency of 12%CO-SOFEC is at least 7% higher than that of SOEC at the current density range of 500 - 2500 A.m<sup>-2</sup>. However, the difference between CO-SOFEC and SOEC decreases at the

current density of over 2500 A.m<sup>-2</sup> due to rapidly increasing concentration overpotential of CO-SOFEC. Without considering the heat input, CH<sub>4</sub>-SOFEC has distinct advantage over the other 2 systems. Fig. 6 shows the efficiency of 12%CH<sub>4</sub>-SOFEC is at least 30% higher than 12%CO-SOFEC and SOEC. When V=0, the efficiencies of CO-SOFEC and CH<sub>4</sub>-SOFEC are 0.88 and 1.24, respectively.

**Table 11 The energy efficiency without considering heat**

**Fig. 6 The efficiency ignoring heat of SOEC, CO-SOFEC and CH<sub>4</sub>-SOFEC**

4.2.3.2 The efficiency considering heat

Heat demand of steam electrolysis becomes more significant with increasing temperature (see Fig. 3). It's also necessary to take heat into account and perform a comprehensive efficiency analysis. Firstly, the cell temperature and inlet gas temperature are assumed to be 800°C and independent on how much the heat is released or consumed, and if the overall heat effect in cell is exothermal, the surplus heat is released to the environment and not considered. It's recognized that the heat demand can be partly or even completely provided by the heat generation from irreversible losses. Consequently, the efficiency expressions after considering heat demand are amended and shown in Table 12. The total reaction of CO-SOFEC has a negative entropy change while that of SOEC or CH<sub>4</sub>-SOFEC has a positive one, so CO-SOFEC doesn't demand heat and the efficiency expression remains unchanged. It's found that when heat is considered, CO-SOFEC has a little more distinct

advantage at low hydrogen production rate compared with SOEC. As for CH<sub>4</sub>-SOFEC, the heat demand  $Q_{re}$  is higher than released heat  $Q_{ir}$  when  $0 < V - V_{OCV} < 0.31$ . In the case of 12%CH<sub>4</sub> assisting,  $Q_{ir} < Q_{re}$  when  $-0.4 < V < -0.09$  while  $Q_{ir} > Q_{re}$  when  $V > -0.09$ , so the expression keeps unchanged when  $V \geq 0$ . The corresponding efficiency curves considering heat are shown in Fig. 7. The highest efficiency of 12%CH<sub>4</sub>-SOFEC reaches 1.32 and is achieved at the applied voltage of -0.09V and the current density of 1400 A.m<sup>-2</sup>. 12%CH<sub>4</sub>-SOFEC still has the same advantage in efficiency compared with SOEC, while the efficiency of 12%CO-SOFEC is more superior than SOEC at low current density. As analyzed above, CH<sub>4</sub>-SOFEC is still more efficient than SOEC and CO-SOFEC. Moreover, more heat released in CO-SOFEC can replenish the unavoidable heat loss to environment to maintain cell at a given temperature.

**Table 12 The energy efficiency taking heat into account**

**Fig. 7 The efficiency considering heat of SOEC, CO-SOFEC and CH<sub>4</sub>-SOFEC**

**4.3 Effects of operating conditions on SOFEC**

4.3.1 Comparison between CO-SOFEC and CH<sub>4</sub>-SOFEC

In order to better understand the behaviors of CO-SOFEC and CH<sub>4</sub>-SOFEC, more detailed information on the reaction and transport processes in SOFEC are studied in this section. Fig. 8 shows the electronic current density distributions within anode of 12%CO-SOFEC and 12%CH<sub>4</sub>-SOFEC at 800°C with the applied voltages of -0.1V/0V/0.2V. When the same voltage is applied to 12%CO-SOFEC and

12%CH<sub>4</sub>-SOFEC, higher current density is generated within the anode of CH<sub>4</sub>-SOFEC than CO-SOFEC. Furthermore, the current density approaches constant values near the anode surface. The current density in the anode of CH<sub>4</sub>-SOFEC remains stable in a wider region than CO-SOFEC, which means that CH<sub>4</sub>-SOFEC has less effective electrochemical reaction zone than CO-SOFEC. Near the anode surface, steam reforming of CH<sub>4</sub> is significant and provides CO and H<sub>2</sub> for further electrochemical oxidation.

**Fig. 8 The electronic current density distributions within anode of 12%CO-SOFEC and 12%CH<sub>4</sub>-SOFEC at 800°C with the applied voltages of -0.1V/0V/0.2V**

**Fig. 9 The polarization voltages of anode, electrolyte and cathode at 800°C.**

The polarization overpotentials of anode, electrolyte and cathode have been separated from polarization curves and shown in Fig. 9. The cathode overpotential dominates the performance at low current density. The anode overpotential greatly increases and gradually exceeds cathode overpotential with increasing current density. This phenomenon is caused by the greatly enlarged concentration polarization in thick anode at a high current density while the concentration polarization in very thin cathode is negligibly small. As Fig. 9 shows, CO-SOFEC and CH<sub>4</sub>-SOFEC show similar overpotentials of electrolyte and cathode because of the completely same conditions in cathode and electrolyte and different assisting-fuel in anode. Calculation indicates SOFEC assisted by 12% CO has larger anode overpotential than 12% CH<sub>4</sub> resulting from the differences of activation polarization and concentration polarization, thus, CH<sub>4</sub>-SOFEC has a better performance than CO-SOFEC.

**Fig. 10 The concentration distributions of gaseous CO, H<sub>2</sub>O and CO<sub>2</sub> in anode fed with 12%CO and 12%CH<sub>4</sub> at applied voltages of -0.1V/0V/0.2V**

Furthermore, distributions of gas species and surface species in anode fed with 12%CO and 12% CH<sub>4</sub> at applied voltages of -0.1V/0V/0.2V are presented and discussed. Fig. 10 shows CO/H<sub>2</sub>O concentration distributions in 12%CO-SOFEC and 12%CH<sub>4</sub>-SOFEC. The mechanism adopted in our model has considered steam reforming reactions including reversible water-gas shift reaction (WGSR) and reversible methane steam reforming reaction (MSRR). Anode gas contains 3% H<sub>2</sub>O for reforming assisting-fuel. In CO-SOFEC, CO is relatively abundant and electrochemically oxidized into CO<sub>2</sub>, so CO concentration decreases with increasing distance from the anode surface. WGSR consumes CO and H<sub>2</sub>O rapidly near the anode surface. When approaching the electrolysis zone, WGSR is impeded as H<sub>2</sub>O is generated from electrochemical oxidation of H<sub>2</sub>. However, the effects of steam reforming reactions and electrochemistry are more complicated in CH<sub>4</sub>-SOFEC. CO is generated by methane partial oxidation(steam reforming reaction), thus, CO concentration increases with increasing distance from the anode surface. H<sub>2</sub>O in the anode of CH<sub>4</sub>-SOFEC is much more insufficient than that in the anode of CO-SOFEC. Methane is firstly transformed into CO and H<sub>2</sub>, which are electrochemically oxidized. Consequently, if completely transferred by steam reforming, 12% CH<sub>4</sub> can provide more mixture of CO and H<sub>2</sub> than the 12%CO-SOFEC case. Therefore, better performance is obtained when steam electrolysis is assisted by 12% CH<sub>4</sub>. Fig. 11 shows the concentration distribution of surface species. The figure indicates that (Ni),



CO(Ni) and O(Ni) are the major surface species in both CO-SOFEC and CH<sub>4</sub>-SOFEC. In CO-SOFEC, (Ni) increases and CO(Ni) decreases with increasing distance from anode surface. However, the variations of (Ni) and CO(Ni) are opposite in CH<sub>4</sub>-SOFEC. Moreover, Fig. 11(b) indicates C(Ni) is unimportant for CO-SOFEC but significant for CH<sub>4</sub>-SOFEC. The C(Ni) concentration in CH<sub>4</sub>-SOFEC is as much as O(Ni) concentration and 3-4 orders of magnitude higher than that in CO-SOFEC, implying the significance of carbon deposition in CH<sub>4</sub>-SOFEC.

**Fig. 11 The concentration distributions of surface species in anode fed with 12%CO and 12%CH<sub>4</sub> at applied voltages of -0.1V/0V/0.2V:a) (Ni)/CO(Ni)/CO<sub>2</sub>(Ni); b) C(Ni)/O(Ni).**

#### 4.3.2 Effect of anode gas composition

As discussed above, anode concentration polarization plays a significant role in the irreversible losses of SOFEC. The anode gas composition is changed and results are compared. Fig. 12 shows the polarization and efficiency curves with different molar fractions of CO or CH<sub>4</sub>. From Fig. 12(a), it is found that higher molar fraction of fuel is helpful to improve the cell performance of CO-SOFEC at an applied voltage of above zero. In these two cases, similar performances and efficiencies are obtained when current density is less than 1000A.m<sup>-2</sup>(V<0) owing to relatively low CO consumption rate (equal to H<sub>2</sub> production rate). With an increase in current density and CO consumption rate, concentration polarization of SOFEC assisted by 12% CO increases rapidly, resulting in much lower performance than SOFEC assisted with higher CO concentration. When the efficiency is 0.7, the current density of

48%CO-SOFEC ( $5000\text{A.m}^{-2}$ ) is 66.7% higher than that of 12%CO-SOFEC ( $3000\text{A.m}^{-2}$ ).

Because carbon deposition is unavoidable when high molar fraction of  $\text{CH}_4$  is used in SOFEC, 12% and 3%  $\text{CH}_4$ -assisted SOFECs are chosen for comparison as shown in Fig. 12(b). Similarly, higher molar fraction of  $\text{CH}_4$  brings better cell performance of  $\text{CH}_4$ -SOFEC. At low current density (below  $700\text{ A.m}^{-2}$ ), 3%  $\text{CH}_4$ -assisting SOFEC has a relatively higher efficiency because the heat generation from polarization losses meets the heat demand. However, 12%  $\text{CH}_4$ -assisted SOFEC achieves an over 10% higher efficiency than 3%  $\text{CH}_4$ -assisted one at high current density. When the efficiency is 1.1, the current density of 12%  $\text{CH}_4$ -SOFEC ( $2600\text{A.m}^{-2}$ ) is 48.6% higher than that of 3%  $\text{CH}_4$ -SOFEC ( $1750\text{A.m}^{-2}$ ).

**Fig. 12 The polarization and efficiency curves of SOFEC a) assisted by 12%/48% CO; b) assisted by 3%/12%  $\text{CH}_4$**

#### 4.3.3 Effect of applied voltage

The effects of operating voltage can also be seen from Fig. 12. Obviously, increasing the applied voltage considerably increases the current density and the rate of hydrogen generation. Even for  $\text{CH}_4$ -SOFEC, the heat released from irreversible losses is far more than the reversible heat demanded at high current density. Therefore, if higher hydrogen production rate is needed, higher voltage should be applied, which in turn cause larger irreversible losses and lower efficiency. In practice, an appropriate applied voltage can be determined after considering both efficiency and hydrogen

demand. When applied in larger scale, such as cell units or SOFEC system, fuel utilization neglected in this button cell model should be also considered.

## 5. Conclusion

In this paper, a one-dimension elementary reaction kinetic model for solid oxide fuel-assisted steam electrolysis cell(SOFEC) is developed coupling heterogeneous elementary reactions, electrochemical reaction kinetics, electrode microstructure and transport processes of charge and mass. This model is well calibrated and validated by experimental data from a button cell with anode gases of H<sub>2</sub>, CO and CH<sub>4</sub> at 800°C.

On the basis of model assumptions, the energy demands, performance and efficiency are analyzed to compare CO/CH<sub>4</sub>-assisted SOFEC with SOEC. Whether heat consumption is considered, SOFEC is found to have better performance and higher efficiency than SOEC, especially at low current density. Thereinto, CH<sub>4</sub>-SOFEC is superior to CO-SOFEC. Efficiency analysis indicates the efficiency of CH<sub>4</sub>-SOFEC is at least 30% higher than CO-SOFEC and SOEC when the current density is below 3300 A.m<sup>-2</sup>. When considering heat, 12%CH<sub>4</sub>-SOFEC has the highest efficiency of 1.32 at the current density of 1400 A.m<sup>-2</sup>. If the hydrogen production doesn't require too fast, CO-SOFEC is still significantly superior in efficiency to SOEC.

In addition, the effect of type of assisting-fuel, fuel composition and applied voltage are studied. It indicates that CO-SOFEC has higher anode polarization leading

to worse performance than CH<sub>4</sub>-SOFEC with the same molar fraction of fuel. Moreover, the mechanism shows CH<sub>4</sub> is not directly electrochemically oxidation but transferred by steam reforming to CO and H<sub>2</sub> for further electrochemical oxidation. Therefore, steam reforming of CH<sub>4</sub> is pretty significant, by which CH<sub>4</sub> can provide more mixture of CO and H<sub>2</sub> than the same molar fraction of CO to obtain better performance and higher efficiency. Moreover, C(Ni) is unimportant for CO-SOFEC but significant for CH<sub>4</sub>-SOFEC implying carbon deposition is a significant problem in CH<sub>4</sub>-SOFEC. At high current density, the lack of assisting fuel leads to SOFEC increasing overpotentials and decreasing efficiency, which can be alleviated by using higher proportion of fuel. The current density of 48%CO-SOFEC is 66.7% higher than that of 12%CO-SOFEC at the efficiency of 1.1, while the current density of 12% CH<sub>4</sub>-SOFEC is 48.6% higher than that of 3% CH<sub>4</sub>-SOFEC at the efficiency of 1.1.

## **Acknowledgements**

The study was supported by Project 51276098 supported by the Natural Science Foundation of China (NSFC), Project 2014CB249201 supported by the National Basic Research Program of China (973 Program), Doctoral Fund of Ministry of Education of China (No. 20110002120017), and a fund from the Hong Kong Research Grant Council (No. PolyU 5326/12E).

## **Reference**

- 
- [1] Ni M, Leung M K H, Leung D Y C. Technological development of hydrogen production by solid oxide electrolyzer cell (SOEC). *International Journal of Hydrogen Energy* 2008;33:2337 54.
- [2] Martinez-Frias J, Pham A Q, Aceves M. A natural gas-assisted steam electrolyzer for high-efficiency production of hydrogen. *International Journal of Hydrogen Energy* 2003;28: 483 90.
- [3] Donitz W, Edle E, Streicher R. In: Wendt H, editor. *Electrochemical hydrogen technologies*. Amsterdam: Elsevier, 1990. p. 213.
- [4] Pham AQ, Wallman H, Glass RS. US patent no. 6051125, April, 2000.
- [5] Wang W, Vohs J M, Gorte R J. Hydrogen production via CH<sub>4</sub> and CO assisted steam electrolysis. *Topics in Catalysis* 2007;46:380 5.
- [6] Wang W, Gorte R J, Vohs J M. Analysis of the performance of the electrodes in a natural gas assisted steam electrolysis cell. *Chemical Engineering Science* 2008;63: 765 9.
- [7] Tao G, Butler B, Virkar A. Hydrogen and Power by Fuel-Assisted Electrolysis Using Solid Oxide Fuel Cells. *ECS Transactions* 2011;35:2929 39.
- [8] Hecht E S, Gupta G K, Zhu H, Dean A M, Kee R J, Maier L, Deutschmann O. Methane reforming kinetics within a Ni-YSZ SOFC anode support. *Applied Catalysis A: General* 2005;295: 40 51.
- [9] Janardhanan V M, Deutschmann O. CFD analysis of a solid oxide fuel cell with internal reforming: Coupled interactions of transport, heterogeneous catalysis and electrochemical processes. *Journal of Power Sources* 2006;162:1192 202.
- [10] Shi Y, Li C, Cai N. Experimental characterization and mechanistic modeling of carbon monoxide fueled solid oxide fuel cell. *Journal of Power Sources* 2011;196:5526 37.
- [11] Li C, Shi Y, Cai N. Elementary reaction kinetic model of an anode-supported solid oxide fuel cell fueled with syngas. *Journal of Power Sources* 2010;195:2266 82.
- [12] Shi Y, Luo Y, Cai N, Qian J, Wang S, Li W, Wang H. Experimental characterization and modeling of the electrochemical reduction of CO<sub>2</sub> in solid oxide electrolysis cells. *Electrochimica Acta* 2013;88:644 53
- [13] Li W, Shi Y, Luo Y, Cai N. Elementary reaction modeling of CO<sub>2</sub>/H<sub>2</sub>O co-electrolysis cell considering effects of cathode thickness. *J Power Sources* 2013;243:118 30
- [14] Shi Y, Cai N, Li C, Bao C, Croiset E, Qian J, Hu Q, Wang S. Modeling of an anode-supported Ni-YSZ|Ni-ScSZ|ScSZ|LSM-ScSZ multiple layers SOFC cell: Part I. experiments, model development and validation. *J Power Sources* 2007;172:235 45
- [15] Shi Y, Cai N, Li C, Bao C, Croiset E, Qian J, Hu Q, Wang S. Modeling of an anode-supported Ni-YSZ|Ni-ScSZ|ScSZ| LSM-ScSZ multiple layers SOFC cell: Part II. simulations and discussion. *J Power Sources* 2007;172:246 52
- [16] Costamagna P, Costa P, Antonucci V. Micro-modelling of solid oxide fuel cell electrodes. *Electrochimica Acta* 1998;43:375 94.
- [17] Chan S H, Xia Z T. Anode micro model of solid oxide fuel cell. *Journal of the Electrochemical Society* 2001;148:A388 94.
- [18] Kee R J, Coltrin M E, Blarborg P. *Chemically Reacting Flow*. John Wiley & Sons. 2003.
- [19] Bieberle A, Gauckler L J. State-space modeling of the anodic SOFC system Ni, H<sub>2</sub>-H<sub>2</sub>O | YSZ. *Solid State Ionics* 2002;146:23 41.
- [20] Zhang Y, Xia C, Ni M. Simulation of sintering kinetics and microstructure evolution of composite solid oxide fuel cells electrodes. *International Journal of Hydrogen Energy* 2012;37:3392 402.
- [21] Zhang Y, Sun Q, Xia C, Ni M. Geometric properties of nanostructured solid oxide fuel cell electrodes. *Journal of the Electrochemical Society* 2013;160:F278 89.
- [22] Zhang Y, Ni M, Xia C. Microstructural Insights into Dual-Phase Infiltrated Solid Oxide Fuel Cell Electrodes. *Journal of the Electrochemical Society* 2013;160:F834 9.
- [23] Chan S H, Chen X J, Khor K A. Cathode micromodel of solid oxide fuel cell. *Journal of the Electrochemical Society* 2004;151:A164 72.
- [24] Mason E A, Malinauskas A P. *Gas transport in porous media: the dusty-gas model*. Amsterdam: Elsevier, 1983.
- [25] Todd B, Young J B. Thermodynamic and transport properties of gases for use in solid oxide fuel cell modelling. *Journal of Power Sources* 2002;110:186 200.
- [26] Nagata S, Momma A, Kato T, Kasuga Y. Numerical analysis of output characteristics of

---

tubular SOFC with internal reformer. Journal of Power Sources 2001;101:60 71.  
[27] Divisek J, Wilkenhöner R, Volkovich Y. Structure investigations of SOFC anode cermets  
Part I: Porosity investigations. Journal of Applied Electrochemistry 1999;29:153 63.  
[28] Serway R, Raymond A. Principles of Physics. Fort Worth, Texas; London: Saunders College  
Pub. 1998 p.602.